ANALYSIS OF HEAT TRANSFER MECHANISMS IN MICROCHANNELS WITH DIFFERENT VORTEX-INDUCING MICROSTRUCTURES

Xuechun WAN**, **Ding YUAN*, ***Zhiyong CHE**, **Zhujun LI**,* **Yifei *LIU*, Jincai *ZHU***

School of Mechanical and Electrical Engineering, Guangzhou Railway Polytechnic, Guangzhou 511300, China.

* Corresponding author; Email: stu_yuand@163.com

In this study, the flow characteristics and heat transfer mechanism of longitudinal vortices induced by a microchannel containing double-row rib microstructures (DLM), a microchannel containing single-row rib microstructures (SLM), and a smooth microchannel (SM) were comprehensively analyzed through numerical simulations at Reynolds numbers (Re) of 164-965. It was found that the SLM had the highest Nusselt number Nu (Nu=28) and the best comprehensive evaluation factor (PEC) (PEC=2.1). The study revealed that the primary mechanism for enhancing heat transfer in SLM was the disruption of the thermal boundary layer. This led to improved heat transfer performance in SLM, despite its fewer longitudinal vortices compared to DLM. Flow analysis revealed that the formation of two longitudinal vortices created a lubrication-like effect in DLM. Consequently, the pressure drop observed in DLM was 28% lower than that in SLM, and the intensity of the vortices was also found to be less than that of SLM.

Keywords: microchannel, longitudinal vortices, thermal-hydraulic characteristics, heat transfer enhancement.

1 Introduction

With the rapid advancement of modern electronic technology, the heat flux of microprocessors, integrated circuits, and other electronic components has increased significantly. Consequently, the issue of heat dissipation has emerged as a critical factor that limits the enhancement of their performance [1]. Microchannel heat dissipation technology is extensively utilized in high-performance computing, aerospace, and biomedical fields, owing to its superior heat dissipation efficiency. However, traditional microchannel designs encounter significant challenges when they are subjected to extremely high heat loads. Consequently, enhancing the heat transfer efficiency of these systems has emerged as a prominent area of research [2].

The formation and evolution of longitudinal vortices, a significant phenomenon in fluid dynamics, exert a profound influence on the flow and heat transfer processes occurring within microchannels. Vortices promote fluid disturbances and facilitate heat transfer from the wall to the fluid body, thereby enhancing overall heat transfer efficiency [3]. Researchers have discovered that longitudinal vortices can disrupt the fluid boundary layer, enhance fluid mixing, and promote heat transfer. By incorporating a longitudinal vortex within the microchannels, the heat-transfer performance of these microchannels can be significantly improved. However, it is important to note that the introduction of longitudinal vortices also increases the flow resistance, which may negatively affect the comprehensive heat transfer efficiency [4].

Currently, research on the impact of longitudinal vortices on the heat transfer in microchannels primarily encompasses two key areas: experimental investigations and theoretical analyses. Experimental research is the most direct and effective approach for validating the effects of longitudinal vortices on heat transfer within microchannels. Researchers have developed microchannels with various geometries, including rectangular, triangular, and trapezoidal. They also incorporated longitudinal vortex generators of differing quantities and configurations to investigate the impact of longitudinal vortices on heat transfer performance. For example, Ebrahimi [5] conducted experiments to investigate the thermal and pressure drop characteristics of water flow in a rectangular microchannel equipped with a longitudinal vortex generator. The study revealed that a longitudinal vortex generator can significantly enhance the heat transfer performance; however, it also leads to an increase in the friction factor. Similarly, Liu *et al*. [6] conducted experimental studies to investigate the effects of longitudinal vortex generators (LVGs) in rectangular microchannels on the fluid flow and heat transfer. Their findings revealed that the heat-transfer performance significantly improved with an increase in the number of LVGs within a certain range; however, this enhancement leveled off beyond a specific threshold. The experimental results indicate that longitudinal vortices significantly influence the thermal performance of microchannels. However, there exists an optimal range within which the enhancement in thermal performance becomes less pronounced beyond this threshold.

Numerical simulation studies, which complement experimental investigations, can offer profound insights into the mechanisms by which longitudinal vortices influence heat transfer in microchannels. Researchers have developed mathematical models for fluid flow and heat transfer within these microstructures and have employed computational fluid dynamics (CFD) techniques to simulate and optimize the behavior of longitudinal vortices. For example, Zhang *et al*. [7] conducted numerical simulations of microchannels with longitudinal vortex generators and analyzed the effects of the length, width, longitudinal spacing, and number of longitudinal vortex generators on the flow and heat transfer performance under different Reynolds numbers. The results showed that the number and vertical spacing of LVGs were the main factors affecting Nu, whereas the number and length of LVGs were the main influencing parameters for flow resistance. Furthermore, some researchers used numerical simulation methods to study the influence of different shapes and sizes of longitudinal vortex generators on the heat transfer performance of microchannels, providing a theoretical basis for the optimization design of longitudinal vortex generators. Datta *et al*. [8] conducted numerical studies on heat transfer and fluid flow processes in microchannels with different LVG angles and reported that the LVG with an attack angle of 30° showed the best overall performance when the Reynolds number was greater than 600.

Researchers have proposed various optimization strategies to improve the heat transfer performance of microchannels. On the one hand, by changing the shape, size, and arrangement of the longitudinal vortex generators, the precise control of the number of longitudinal vortices can be achieved. For example, by using arc-shaped, triangular, and other shapes of longitudinal vortex generators, more longitudinal vortex structures can be generated, thereby enhancing the heat transfer effect [9]. Fu *et al*. [10] studied the effects of the LVG configuration and channel aspect ratio on the heat transfer on a wall, where the LVG geometry and channel height mainly affected the main vortex flow behavior downstream of the LVGs, while having little effect on the vortex structures near the LVGs. On the other hand, by using intelligent optimization algorithms, such as genetic algorithms and neural network algorithms, it is possible to perform global optimization search for the longitudinal vortex and find the optimal longitudinal vortex distribution scheme. Datta *et al*. [11] obtained expressions for the Nusselt number, friction coefficient involving the Reynolds number, and position of the vortex generator using a genetic algorithm. The prediction model showed that the heat transfer performance of the vortex generator was improved by 40-135% compared to a smooth channel, while the pressure drop increased by 62-186.7% as the Reynolds number increased. Esmaeilzadeh *et al*. [12] obtained the optimal geometric parameters for an LVG using neural-network algorithms. Additionally, some researchers proposed combining a longitudinal vortex generator with other heat dissipation technologies, such as nanofluid-enhanced heat transfer technology, to further enhance the heat transfer performance of the microchannel.

Despite the significant progress in recent studies on the influence of longitudinal vortices on microchannel heat transfer, there are still some shortcomings. Current studies mainly focus on the effects of the shape, size, and structural parameters of the longitudinal vortex generator on the heat transfer efficiency and flow resistance. However, there is a lack of in-depth understanding of the influence mechanism of the number and interaction of longitudinal vortices on heat transfer performance. Therefore, this study compares the flow and heat transfer effects of single and double longitudinal vortices to provide a theoretical basis for optimizing the design of microchannel heat dissipation technology.

2 Numerical simulation

2.1 Geometry Models

Fig. 1(a) shows the dimensions of the DLM with a hydraulic diameter (D_h) of 1 mm, width of 1.5 mm, height of 0.75 mm, and wall thickness of 0.5 mm. Both the inlet and outlet were equipped with a 4 mm smooth section. In the central section, there are three sets of double-row ribs (microstructured section), each measuring 8.5 mm in length, with a 2 mm spacing between sets (transitional section). Within each set, the spacing between double-row ribs was 1 mm. Each pair of double-row ribs consisted of two inclined ribs, each with a 45° angle with flowing direction, spaced 0.15 mm apart, and with a rib height of 0.25 mm.

Fig. 1(b) illustrates the geometry of the SLM, which consists of single-row ribs. The length of a single-row rib was equal to that of a double-row rib. The fluid channel dimensions of the SLM as well as the position and spacing of the single-row ribs were identical to those of the double-row ribs in the DLM. The calculations show that the heat transfer area of the DLM is approximately 15% larger than that of the SLM. Subsequent research revealed that despite the larger heat transfer area of the DLM, its heat transfer performance was lower than that of SLM.

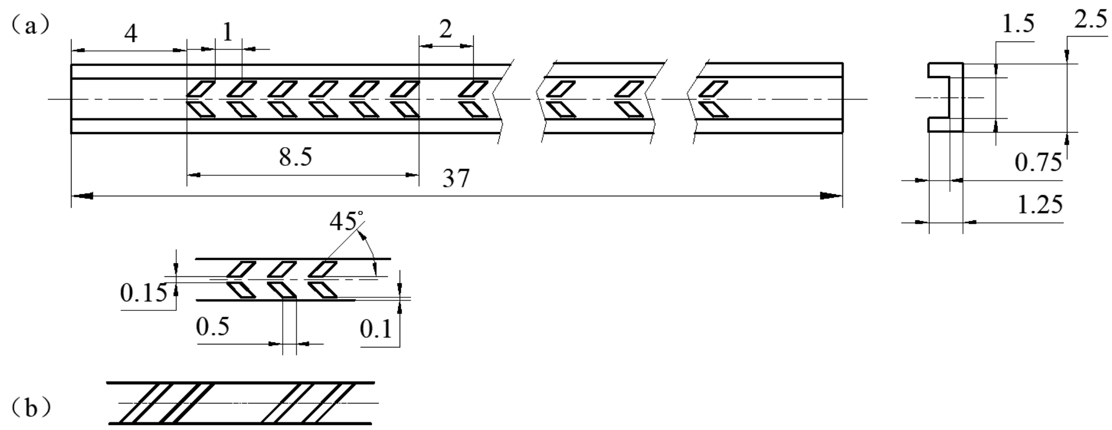

Figure 1. Geometries of different microchannels (unit of mm): (a) DLM and (b) SLM.

2.2 Numerical model

The numerical model was assumed to be a three-dimensional steady-state incompressible laminar flow process, with negligible effects of body forces, gravity, thermal radiation, and viscous dissipation [13]. Based on these assumptions, the governing equations were referenced from the literature [13]. The materials used for SLM and DLM were copper, and deionized water was used as the cooling fluid. The viscosity of deionized water was assumed to vary with temperature fluctuations, and the specific expression was referenced from [14].

The inlet temperature T_{in} of deionized water was 25 °C, and the heat flux q_w applied to the SLM and DLM was 100 kW/m^2. The q_w and T_{in} remained constant, while the inlet flow rate u_{in} of the deionized water uniformly increased from 0.12 m/s to 0.84 m/s with a step of 0.12 m/s. The remaining walls were designated as adiabatic walls without velocity slip. Fluent CFD software was used to solve the model, with the convergence residual set to 10^{-5}.

2.3 Data reduction

The Reynolds number (*Re*), hydraulic diameter of the microchannel (D_h), average Nusselt number (*Nu*) and pressure drop (ΔP) between the inlet and outlet.

To evaluate the overall performance of different microchannels, this study adopts Performance Evaluation Criteria (PEC) [15] for assessment. For this purpose, a comprehensive performance evaluation factor (PEC) is introduced, defined as the ratio of the heat transfer coefficient of the microchannel embedded with microstructures to that of a smooth microchannel under identical pumping power consumption. The PEC is expressed as Equation (1):

$$PEC = \frac{Nu/Nu_0}{(f/f_0)^{1/3}} \tag{1}$$

To evaluate the intensity of the vortex in the cross section of the fluid, the dimensionless secondary flow intensity *Se* is defined as follows:

$$Se = \frac{\rho_f D_h U_s}{\mu_f}, \quad U_s = D_h J_{ABS}^n \tag{2}$$

Where ρ_f is the fluid density, μ_f is the fluid viscosity, and U_s represents the secondary flow velocity, and J_{ABS}^n represents the average angular velocity of the fluid rotating around the main flow direction as the axis.

$$J_{ABS}^{n} = \frac{1}{A(x)} \iint_{A(x)} |\omega^n| \, dA \tag{3}$$

where ω^n and $A(x)$ are the vorticity and cross section of the fluid in the mainstream direction, respectively. Substituting Equation (3) into Equation (2) yields Equation (4), which gives the expression for Se.

$$Se = \frac{\rho_f D_{\mathrm{h}}^2 \frac{1}{A(x)} \iint_{A(x)} |\omega^n| dA}{\mu_{\mathrm{f}}} \tag{4}$$

The ΔSe is the difference between the Se and the Se_{Plain}, where Se and Se_{Plain} stands for the dimensionless secondary flow intensity of microchannels with microstructures and a smooth microchannel, respectively.

$$\Delta Se = Se - Se_{\mathrm{Plain}} \tag{2}$$

2.4 Grid independence

The effects of the grid number on the simulation results are discussed in this section. Based on the boundary conditions in Section 2.2, the numerical average Nusselt number Nu and pressure drop ΔP of the SLM were simulated. As the deviations of ΔP in the SLM corresponding to 0.8 and 1.8 million grids from that corresponding to 1.5 million grids were 7.2% and 2.3%, and the deviations of Nu were 5.3 % and 1.5 %, respectively. The 1.5 million grid number was selected to divide all microchannel geometric models. The discrepancy between the experimental and numerical mean Nu and ΔP of the SLM is validated in Section 2.5.

2.5 Experimental validation

The experimental setup used in this study is described in a previous study [16]. Fig. 2 (a) and (b) present the experimental and numerical simulation results for the average Nusselt number Nu and pressure drop ΔP for the DLM and SLM, respectively. The numerical simulation results of Nu and ΔP were within 10% deviations from their respective measured data, indicating the reliability of the numerical simulation results.

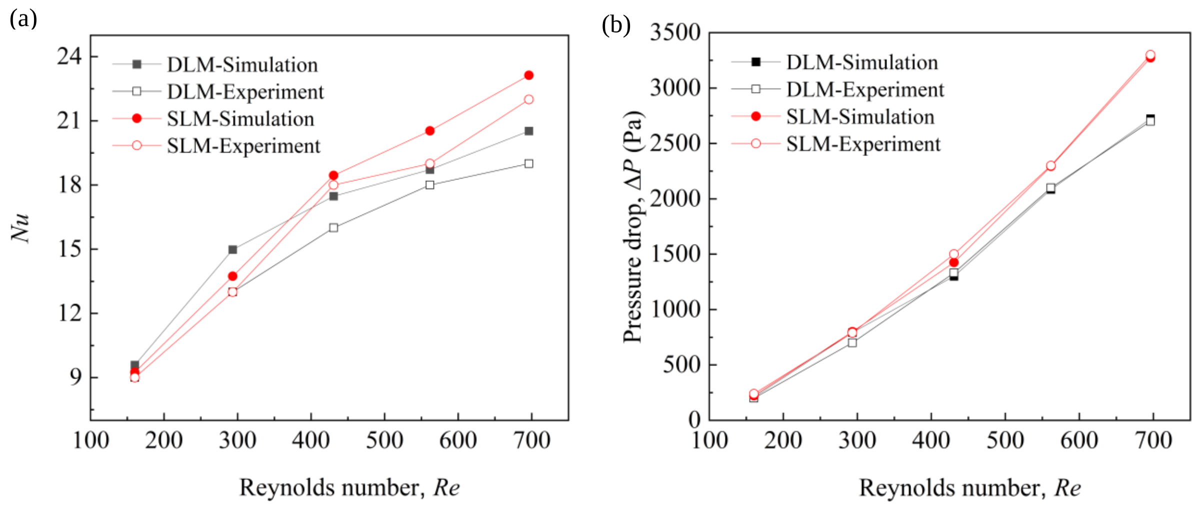

Figure 2. Experimental and numerical simulation studies of DLM and SLM at different Re values: (a) Nu and (b) ΔP.

3 Results and Discussions

3.1 Heat transfer performance

Fig. 3(a) shows that the *Nu* values of SLM and DLM are significantly higher than those of SM, with SLM having a larger *Nu* value than DLM under the same *Re*. This indicates that the single longitudinal vortices induced by the SLM exhibits better heat transfer performance than the double longitudinal vortices induced by the DLM. Fig. 3(b) shows the variation curve of the Nu_x with x. It can be seen that the Nu_x of SM initially increases, then exhibits periodic fluctuations, and eventually slowly declines. This is due to the fact that SM is a smooth microchannel. Consequently, its Nu_x gradually decreases and approaches a constant value as the distance x increases. Comparative analysis demonstrates that both DLM and SLM configurations achieve significantly higher Nu_x values (2.5-3.5 times enhancement) than SM, confirming the heat transfer augmentation effect of longitudinal vortices. Furthermore, the SLM exhibits 15-20% higher Nu_x values than DLM (Re = 500-900), revealing that single longitudinal vortices provide more effective heat transfer enhancement than their double-vortex counterparts.

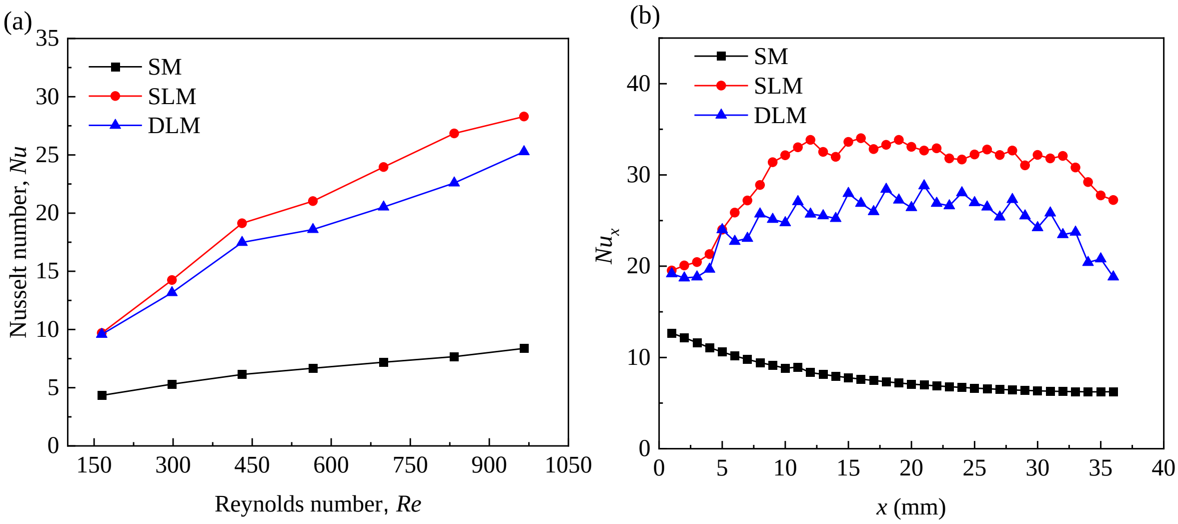

Figure 3. Heat transfer performances of different types of microchannels at u_{in}=0.72 m/s, curves of (a) *Nu* with *Re,* and (b) Nu_x with x at u_{in}=0.72 m/s, Re=833.

3.2 Pressure Drop

Fig. 4 illustrates the flow characteristics of the different types of microchannels. Fig. 4(a) shows the variation in ΔP with *Re*. At the same *Re*, ΔP in the SLM and DLM was significantly higher than that in the SM. This is attributed to the microstructures increasing the variation in fluid velocity, resulting in a higher flow resistance and energy dissipation through vortices. As shown in fig. 4(a), with increasing *Re*, the ΔP between the SLM and DLM compared to the SM becomes more pronounced. This is due to the enhanced vortices with higher flow velocities, which increase flow resistance. Fig. 4(b) shows the variation in pressure along the flow direction (P_x). It is evident from fig. 4(b) that P_x decreases progressively from the inlet to the outlet, with SLM exhibiting a greater pressure variation than DLM, and the inlet pressure of SLM being approximately 1000 Pa higher than that of DLM (higher about 28%). When x increases from 4 to 5 mm, the fluid enters the first set of microstructures, leading to a rapid drop in pressure for SLM and DLM, followed by a fluctuating decrease. This was due to the disturbances induced by the microstructures.

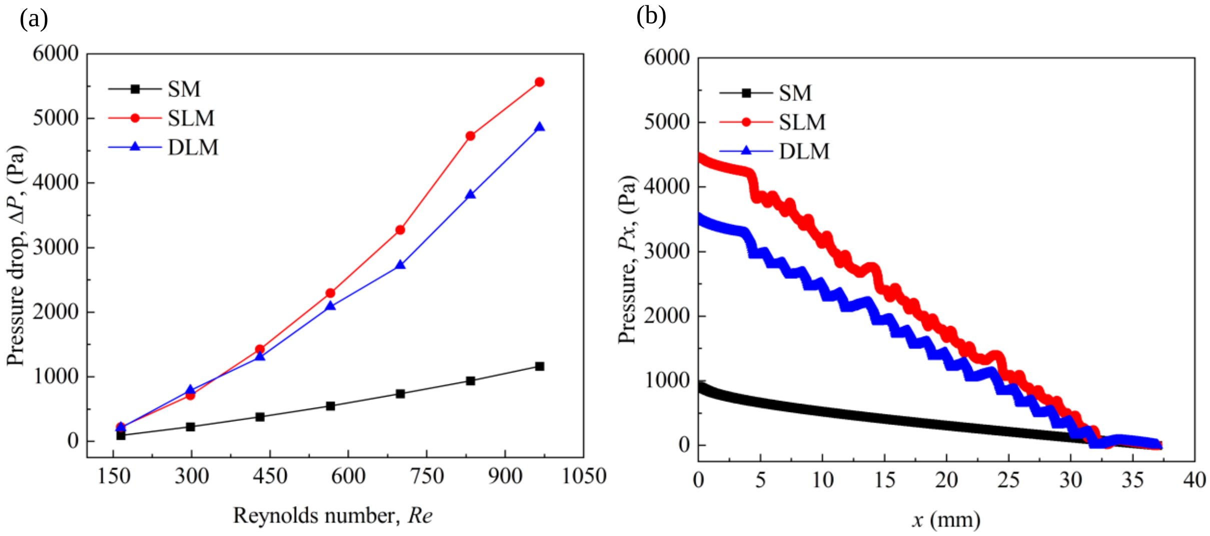

Figure 4. Pressure drop variation in different types of microchannels (a) ΔP with Re, (b) P_x with x, at u_{in}=0.72 m/s, Re=833.

3.3 Vortex intensity

Fig. 5 illustrates the variation curve of the nondimensional flow intensity ΔSe along the flow direction for various types of microchannels. The results reveal that the ΔSe of the SLM is consistent with that of the DLM along the flow direction, yet the ΔSe of the SLM is higher than that of the DLM. When x ranges from 0 to 8 mm, the fluid traverses the smooth and the first microstructured sections. At these sections, the ΔSe of the DLM and SLM increased sharply. As x increases from 9 to 13 mm, ΔSe tends to decline because the fluid is in transition between the first and second microstructured section. As the fluid entered the second microstructured section, ΔSe gradually increased. Due to the interlacing configuration of the microstructured and transitional sections, the secondary flow intensity exhibits fluctuations. Subsequently ($9 \leq x \leq 13$ mm), ΔSe declines in the transitional section between microstructured sections, followed by gradual recovery upon entering the second microstructured section. The alternating transitional sections induce ΔSe fluctuations in both SLM and DLM. Notably, ΔSe shows only mild attenuation over 9–33 mm, confirming longitudinal vortex stability. However, in the smooth exit region (33–37 mm, dashed circle), ΔSe drops abruptly due to absent microstructure effects. Crucially, SLM maintains higher ΔSe than DLM at exit ($\Delta \approx 500$), demonstrating superior vortex persistence and correspondingly enhanced heat transfer efficiency.

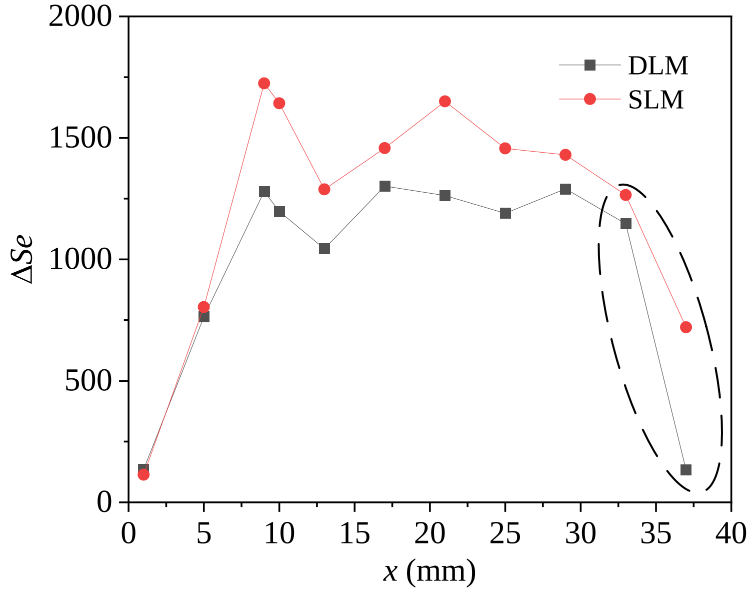

Figure 5. The variation curve of the secondary flow intensity ΔSe of various types of microchannels along the x-axis with u_{in} = 0.72 m/s, Re=833.

3.4 Relationship between flow characteristics and heat transfer

Fig. 6 presents the flow characteristics of different microchannels and clarifies the drag reduction mechanism associated with the DLM, as well as the enhanced heat transfer mechanism related to the SLM. Fig. 6(a), (b), and (c) show the streamlines for the SM, DLM, and SLM, respectively. Fig. 6(a) indicates that the streamlines in the SM were parallel to the flow direction, resulting in poor convective heat transfer. In contrast, fig. 6(b) and (c) reveal that the DLM and SLM generated double longitudinal vortices and a single longitudinal vortex, respectively, demonstrating significant convection. In the SLM, the coolant was directed towards the sidewall by the longitudinal vortex. Fig. 6(b) shows that the double longitudinal vortices in the DLM exhibit an approximately symmetric pattern, similar to that of the two rolling bearings. It suggested that when the secondary flow takes on a "bearing" shape, it effectively separates the main flow region from direct contact with the wall, thus leading to a reduction in flow resistance. In contrast, the SLM exhibits significantly higher flow resistance compared to the DLM. The reason is more obstruction of microchannel because of the existence of fully attached microstructures on fluid path, which leads to more increase in pressure drop. Furthermore, Figures 6(d) and 6(e) demonstrate that while the velocity distributions of both SM and DLM in the z=1.25 mm cross-section remain relatively uniform, the SLM exhibits irregular peripheral velocity divergence. This observation indicates that SM and DLM experience smaller velocity variations compared to SLM.

To further expound on the correlation between flow and heat transfer within various microchannels, from the perspective of convection and heat transfer, it can be discerned in fig. 6 (b) and (c) that the double longitudinal vortices in the DLM exert less influence on the walls on either side of the microchannel; conversely, the single longitudinal vortices in SLM do have an impact on the walls on both sides. This implies that the single longitudinal vortex in SLM exerts a more potent turbulent effect on the wall than the double longitudinal vortex in DLM and has a more substantial effect on disrupting the thermal boundary layer, thereby giving rise to the superior heat transfer effect of SLM. Fig. 6 (d) and (e) reveal that the velocity vectors of SM and DLM are confined to this plane at z = 1.25 mm. In contrast, fig. 6 (f) demonstrates that SLM exhibits a distinct out-of-plane velocity vector at z = 1.25 mm.

This out-of-plane velocity contributes to the convection occurring on both sides of the microchannel in the z direction. To further illuminate the relationship between flow and heat transfer in various microchannels, the velocity vector diagrams at y = 0.8 mm for various microchannels are depicted in fig. 6 (g), (h), and (i) at xy plane. It can be seen from fig. 6 (g) that the velocity vector was parallel to the plane in the SM microchannel. However, in fig. 6 (h) and (i), it is manifested that DLM and SM have conspicuous out-of-plane velocities, which enhances the convective heat transfer at the top and bottom of the microchannel and leads to higher heat transfer efficiency

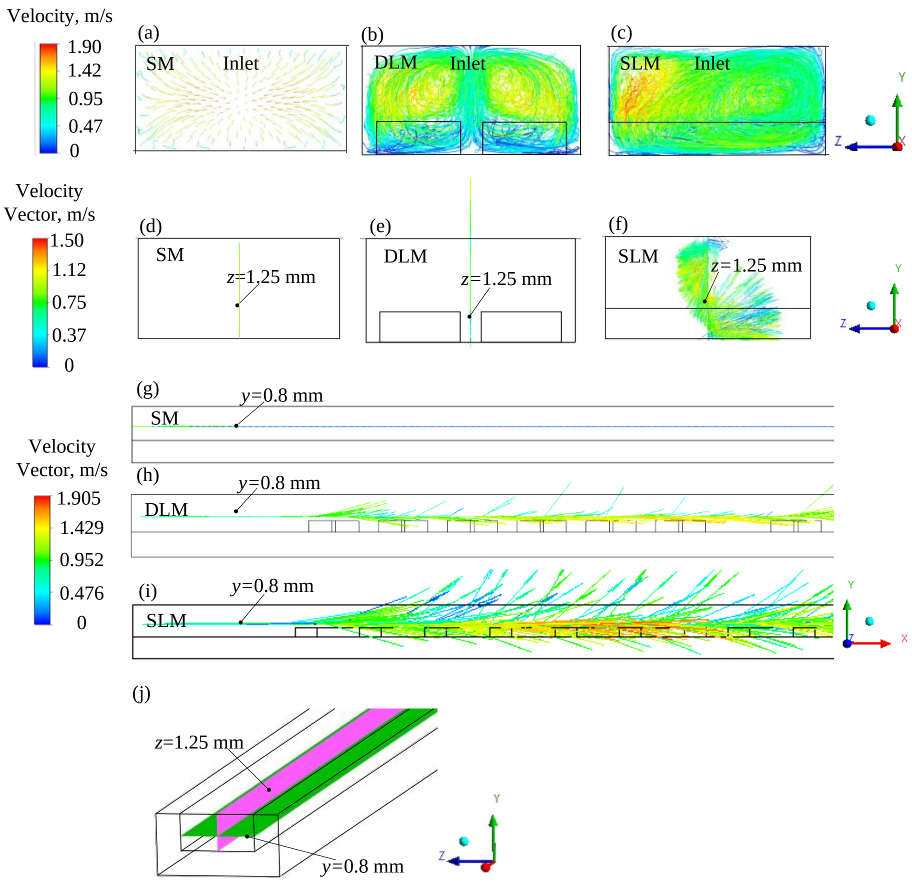

Figure 6. Flow schematics of various microchannels, u_{in} = 0.72 m/s, Re=833, (a), (b), and (c) the velocity vector of SM, DLM, and SLM observed from the inlet respectively; (d), (e), (f) the velocity vector at yz plane; (g), (h), (i) the velocity vector at xy plane; (j) spatial position diagram.

3.5 Heat dissipation characteristic

Figure 7 presents the wall temperature ($T_{w,x}$) distribution along the flow direction in different microchannels. It is evident from figs. 7 (a), (b), and (c) that SM exhibited the highest $T_{w,x}$, followed by DLM and SLM. The $T_{w,x}$ distributions of the CLM and SLM are more uniform, with a much smaller temperature gradient compared to rectangular microchannels, indicating that the DLM and SLM have a superior heat dissipation effect than the SM at the same heat flux and flow rate. Furthermore, figs. 7 (a) and (b) also demonstrate that the $T_{w,x}$ of SLM is lower than that of DLM, suggesting that SLM has a better heat dissipation effect than DLM. The temperature difference between the inlet and outlet of DLM and SLM is approximately 3.1 K and 1.4 K, respectively, while the temperature difference of SM is 13.3 K. This indicates that the $T_{w,x}$ of the SM is highly uneven, in contrast to the SLM and DLM.

Simultaneously, $T_{w,x}$ of SLM is lower than that of DLM, suggesting that SLM has a superior heat dissipation effect than DLM.

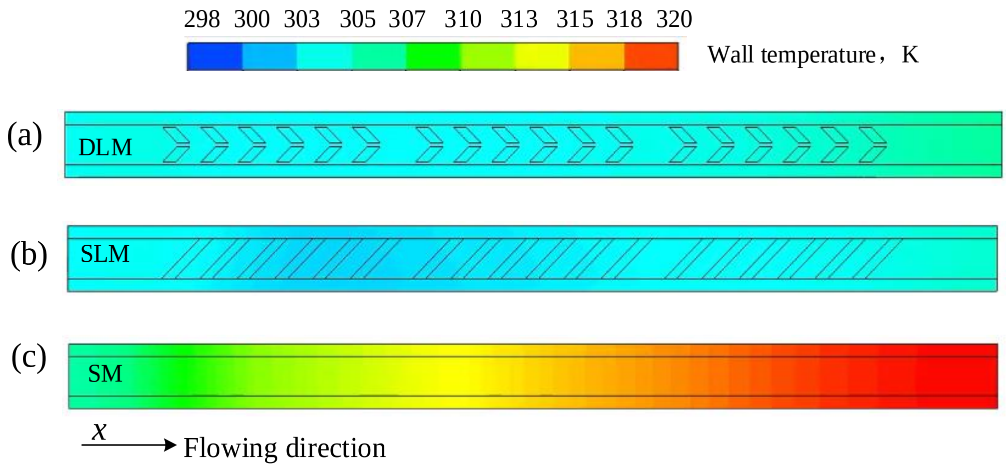

Figure 7. Wall temperature $T_{w,x}$ distribution of different microchannels at u_{in}=0.72 m/s, *Re*=833: (a) DLM, (b) SLM, and (c) SM.

Fig. 8 presents the temperature distribution of the liquids at the exits of the various microchannels. It can be observed from fig. 8 (a), (b), and (c) that DLM and SLM exhibit a more uniform temperature distribution than SM. The thickness of the temperature boundary layer of the SM was significantly greater than that of the DLM and SLM (circled by black dashed lines). The boundary layer thickness of the double longitudinal vortex is greater than that of the single longitudinal vortex. This observation indicates that the disturbance caused by a single longitudinal vortex on the boundary layer is more significant than that produced by a double longitudinal vortex. Consequently, this leads to an improved heat transfer performance in SLM compared to both SM and DLM.

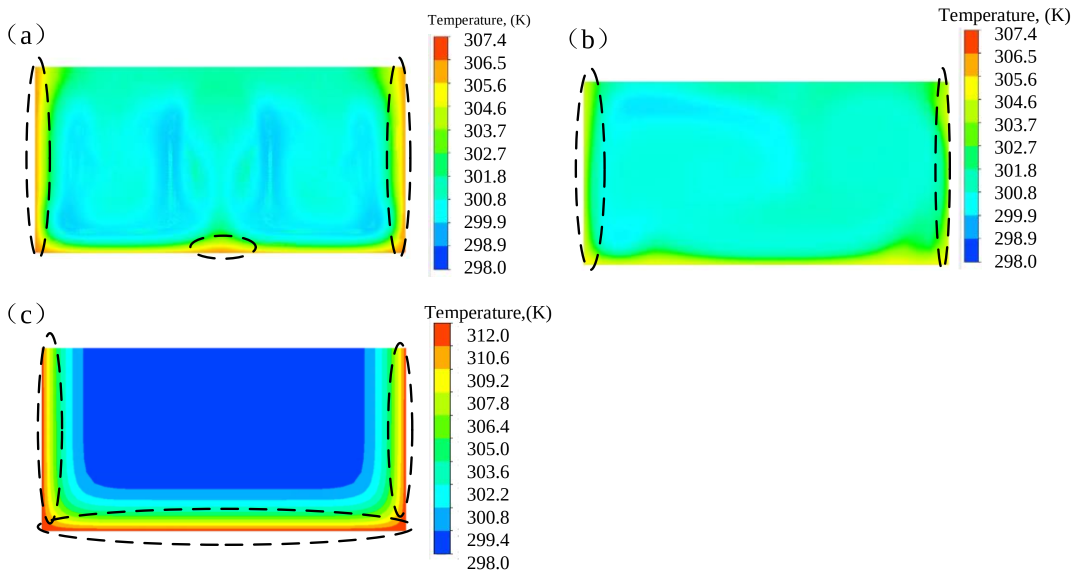

Figure 8. Temperature distribution at various microchannel outlets, u_{in}=0.72 m/s, *Re*=833, (a) DLM, (b) SLM, (c) SM.

3.6 Comprehensive heat transfer performance

Although the ΔP between the inlet and outlet of the DLM is lower than that of the SLM, the *Nu* values for the DLM is also lower than that for the SLM. Therefore, it is crucial to investigate the Comprehensive heat transfer performance (PEC) of both the DLM and SLM. Fig. 9 shows the comprehensive heat transfer factor PEC of DLM and SLM. The findings indicate that when *Re* varies within the range of 150-1000, the PEC of SLM is significantly greater than that of DLM, and the PEC of SLM is superior. The results suggest that single longitudinal vortex is more beneficial for enhancing microchannel heat transfer.

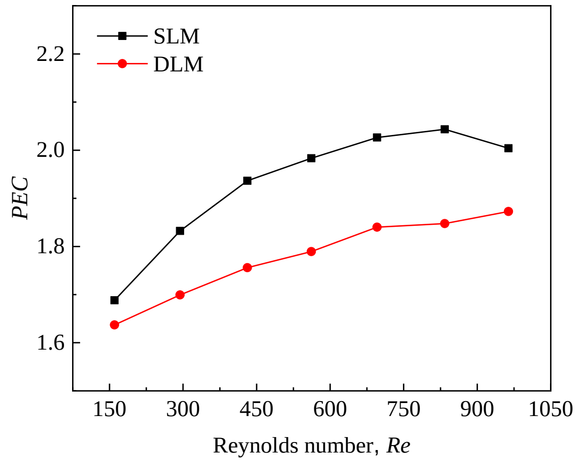

Figure 9. shows the curves of PEC and *Re* for the comprehensive heat transfer performance PEC of the various microchannels.

4. Conclusions

This study aims to investigate the heat transfer performance of double longitudinal vortices and single longitudinal vortices generated by double-row ribs and single-row ribs. The flow characteristics of the DLM and SLM were also examined, leading to the following main conclusions:

(1) In the SLM, the ribs maintain full contact with both sidewalls of the microchannel, creating a obstruction that significantly impedes fluid flow. In contrast, the DLM features gaps between adjacent ribs as well as between the ribs and microchannel walls, allowing partial fluid bypass. As a result, the SLM demonstrates substantially higher flow resistance and elevated pressure drop ΔP compared to the DLM. At a Reynolds number (Re = 833), the ΔP in the SLM was measured to be approximately 28% greater than that in the DLM, highlighting the impact of structural differences on hydrodynamic performance.

(2) Single longitudinal vortices was less prone to decay than double longitudinal vortices, with a higher secondary flow intensity ΔSe in the cross-section of the SLM. The *Nu* and *PEC* values of SLM were higher than that of the DLM 18.8% and 10% at Re=833, respectively.

(3) Disrupting the thermal boundary layers had a greater impact on enhancing the heat transfer performance than increasing the heat transfer area in microchannels.

Acknowledgments

This study was supported by the Newly Introduced Talents Research Project of Guangzhou Railway Polytechnic (GTXYR2303).

References

[1] G.W. Xiahou, R. Ma, J. J. Zhang, S. Zhang and Y. C. He, (2020) “Thermal performance of an array

condenser flat heat pipe for IGBT heat dissipation," Microelectronics Reliability,104, 113546.
[2] J.H. Liu, Z.F. Feng, Z.Z. Li, S.P. Liang, J.C. Nie, Z.Y. Wang, J.X. Zhang, F.W. Guo and D. Yuan, (2024) "Temperature uniformity analysis and multi-objective optimization of the microchannel heat sink with cavities under longitudinal vortex flow," International Journal of Thermal Sciences, 201, 109034.
[3] J. Wang, K. Yu, M.Z. Ye, E. Wang, W. Wang and B. Sunden, (2022) "Effects of pin fins and vortex generators on thermal performance in a microchannel with Al_2O_3 nanofluids," Energy, 239, 122606.
[4] J.S. Yang, M. Jeong, Y.G. Park and M.Y. Ha, (2019) "Numerical study on the flow and heat transfer characteristics in a dimple cooling channel with a wedge-shaped vortex generator," International Journal of Heat and Mass Transfer, 136, 1064-1078.
[5] A. Ebrahimi, E. Roohi and S. Kheradmand, (2015) "Numerical study of liquid flow and heat transfer in rectangular microchannel with longitudinal vortex generators," Applied Thermal Engineering, 78576-583.
[6] C. Chen, J.T. Teng, C.H. Cheng, S.P. Jin, S.Y. Huang, C. Liu, M.T. Lee, H.H. Pan, and R. Greif, (2014) "A study on fluid flow and heat transfer in rectangular microchannels with various longitudinal vortex generators," International Journal of Heat And Mass Transfer, 69, 203-214.
[7] J.F. Zhang, L. Jia, W.W. Yang, J. Taler, and P. Oclon, (2019) "Numerical analysis and parametric optimization on flow and heat transfer of a microchannel with longitudinal vortex generators," International Journal of Thermal Sciences, 141.
[8] A. Datta, A.K. Das, P. Dey and D. Sanyal, (2017) "Multi-objective optimization of laminar heat transfer and friction factor in rectangular microchannel with rectangular vortex generators: an application of NSGA-II with gene expression programing metamodel," Journal of Heat Transfer-Transactions of The ASME, 139, 072401.
[9] A. Mohammadi, A. Kosar, (2018) "Review on Heat and Fluid Flow in Micro Pin Fin Heat Sinks under Single-phase and Two-phase Flow Conditions," Nanoscale and Microscale Thermophysical Engineering, 22, 153-197.
[10] H. Fu, H.O. Sun, L.F. Yang, L.Y. Yan, Y.G. Luan and F. Magagnato, (2023) "Effects of the configuration of the delta winglet longitudinal vortex generators and channel height on flow and heat transfer in minichannels." Applied thermal engineering, 227, 120401.
[11] J.K. Shao, Y.P. Hao and Z.Y.Li, (2024) "Multi-objective optimization of a microchannel heat sink combining cavities and longitudinal vortex generators based on CFD and NSGA-II genetic algorithm," International Journal of Heat and Mass Transfer, 220, 125019.
[12] A. Esmaeilzadeh, N. Amanifard, and H.M. Deylami, (2017) "Comparison of simple and curved trapezoidal longitudinal vortex generators for optimum flow characteristics and heat transfer augmentation in a heat exchanger," Applied Thermal Engineering, 125, 1414-1425.
[13] Z.F. Feng, X.P. Luo, F. Guo, H.Y Li and J.X Zhang, (2017) "Numerical investigation on laminar flow and heat transfer in rectangular microchannel heat sink with wire coil inserts," Applied Thermal Engineering, 116, 597-609.
[14] Z. Dai, Z. Zheng, D.F. Fletcher and B.S. Haynes, (2015) "Experimental study of transient behaviour of laminar fow in zigzag semi-circular microchannels," Experimental Thermal and Fluid Science, 68, 644-651.
[15] D. Yuan, W. Zhou, T. Fu and C. Liu, (2020) "Experimental and numerical investigation ofheat and mass transfer in non-uniform wavy microchannels," International Journal of Thermal Sciences, 152, 106320.
[16] C. Castelain, A. Mokrani, Y.L. Guer and H. Peerhossaini (2001) "Experimental study of chaotic

advection regime in a twisted duct flow," European Journal of Mechanics B-Fluids, 20(2), 205-232.

Paper submitted: 05.04.2025
Paper revised: 15.06.2025
Paper accepted: 23.06.2025